Journal of Sound and Vibration (2002) **251**(5), 919–926
doi:10.1006/jsvi.2001.3906, available online at http://www.idealibrary.com on IDEAL®

LETTERS TO THE EDITOR

USE OF FREQUENCY DATA TO PREDICT SECONDARY BIFURCATION

L. N. VIRGIN

Department of Mechanical Engineering and Materials Science, Duke University, Durham, NC 27708-0300, *U.S.A. E-mail: l.virgin@duke.edu*

AND

R. H. PLAUT

Charles E. Via, Jr. Department of Civil and Environmental Engineering, Virginia Polytechnic Institute and State University, Blacksburg, VA 24061–0105, *U.S.A.*

(*Received* 12 *July* 2001)

1. INTRODUCTION

Changes in measured vibration frequencies during increasing loading have been used to predict critical loads for buckling [1]. It is proposed here that secondary bifurcation also can be predicted using extrapolation of frequency data. As the load is increased, some systems bifurcate at the critical load from a trivial solution to an initially stable post-buckled path, which then becomes unstable when another (secondary) bifurcation point is reached. At secondary bifurcation, the system may suddenly jump to a different shape (mode jumping), which may cause damage. Therefore, the prediction of secondary bifurcation is of practical as well as theoretical interest.

Secondary bifurcation has been examined widely for compressed rectangular plates (e.g., references [2, 3]), often where the secondary bifurcation initiates mode jumping [4]. A simple two-degree-of-freedom system, called Augusti's model, that exhibits similar behavior has been used to study this phenomenon. Quasi-static analyses were carried out in references [5–7] using the full non-linear equations and in references [8–12] using a truncated form of these equations (retaining cubic terms). The aerodynamic response of the model to transverse flow was examined in reference [13].

In the present investigation, free vibrations of Augusti's model about the trivial equilibrium state and the stable post-buckled equilibrium state are considered, using the full non-linear equations. One of the two vibration frequencies reduces to zero at the critical load. Subsequently, the other frequency reduces to zero when secondary bifurcation occurs (and the post-buckled state then becomes unstable). Extrapolation of this second frequency using measured data provides a means for estimating the load at which this instability occurs.

2. FORMULATION

The model is depicted in Figure 1. A slender, rigid bar of length L is pinned at its base, where rotational springs with constant stiffnesses C_1 and C_2 ($C_2 > C_1$) initially act in perpendicular planes and rotate with the bar. The corresponding angles of rotation with

0022-460X/02/$35.00

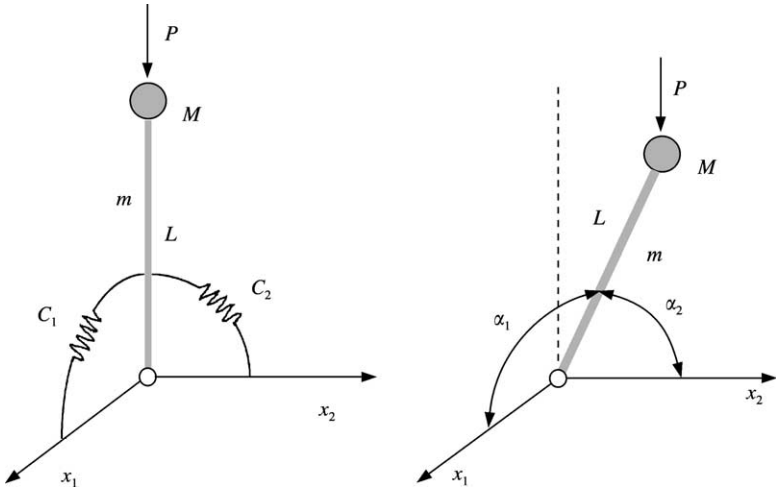

Figure 1. Geometry of model.

respect to two horizontal, perpendicular axes are $\alpha_1(t)$ and $\alpha_2(t)$, and the angles $\theta_1(t)$ and $\theta_2(t)$ are defined as

$$\theta_1(t) = (\pi/2) - \alpha_1(t), \qquad \theta_2(t) = (\pi/2) - \alpha_2(t) \tag{1}$$

with $\theta_1(t) = \theta_{10}$ and $\theta_2(t) = \theta_{20}$ when the springs are unstretched. A downward vertical load P is applied at the top of the bar. A concentrated mass M may be attached at the top of the bar, and the bar is assumed to have a circular cross-section with uniform mass per unit length m and moment of inertia $I = mL^2/3$ about any horizontal axis through its base.

The potential energy V is given by

$$\begin{aligned} V = {} & \tfrac{1}{2}C_1(\theta_1 - \theta_{10})^2 + \tfrac{1}{2}C_2(\theta_2 - \theta_{20})^2 \\ & - PL[(1 - \sin^2\theta_{10} - \sin^2\theta_{20})^{1/2} - (1 - \sin^2\theta_1 - \sin^2\theta_2)^{1/2}] \end{aligned} \tag{2}$$

and the kinetic energy T is

$$T = \tfrac{1}{2}ML^2\left[\left(\frac{\mathrm{d}\theta_1}{\mathrm{d}t}\right)^2\cos^2\theta_1 + \left(\frac{\mathrm{d}\theta_2}{\mathrm{d}t}\right)^2\cos^2\theta_2 + v_3^2\right] + \tfrac{1}{2}I\left[\left(\frac{\mathrm{d}\theta_1}{\mathrm{d}t}\right)^2 + \left(\frac{\mathrm{d}\delta}{\mathrm{d}t}\right)^2\cos^2\theta_1\right], \tag{3}$$

where δ, v_3, and η are defined by [5–7, 14]

$$\begin{gathered} \sin\delta = (\sin\theta_2)/(\cos\theta_1), \qquad v_3 = \eta\left[\left(\frac{\mathrm{d}\theta_1}{\mathrm{d}t}\right)\sin 2\theta_1 + \left(\frac{\mathrm{d}\theta_2}{\mathrm{d}t}\right)\sin 2\theta_2\right], \\ \eta = \tfrac{1}{2}(1 - \sin^2\theta_1 - \sin^2\theta_2)^{-1/2}. \end{gathered} \tag{4}$$

Lagrange's equations are used to obtain the equations of motion.

The non-linear inertia terms in the resulting equations do not affect small vibrations of the system about an equilibrium state. Also, in the responses following small initial

conditions considered in section 5, the non-linear inertia terms have an insignificant effect. Hence, for simplicity, only the linearized inertia terms will be used.

The analysis will be conducted in terms of the following non-dimensional quantities, where Ω is a dimensional vibration frequency:

$$c = \frac{C_2}{C_1}, \qquad p = \frac{PL}{C_1}, \qquad \tau = t\left[\frac{C_1}{I + ML^2}\right]^{1/2}, \qquad \omega = \Omega\left[\frac{I + ML^2}{C_1}\right]^{1/2}, \tag{5}$$

with $c > 1$. The coupled, non-linear equations of motion are obtained as follows:

$$\frac{\mathrm{d}^2\theta_1}{\mathrm{d}\tau^2} + \theta_1 - \theta_{10} - p\eta \sin 2\theta_1 = 0, \qquad \frac{\mathrm{d}^2\theta_2}{\mathrm{d}\tau^2} + c\theta_2 - c\theta_{20} - p\eta \sin 2\theta_2 = 0. \tag{6}$$

3. CHARACTERISTIC CURVES FOR PERFECT SYSTEM

The case $\theta_{10} = \theta_{20} = 0$ is considered in this section, where the bar is vertical when the springs are unstretched, as shown in Figure 1. The equilibrium solutions, determined from equations (6) without the inertia terms, consist of the trivial solution $\theta_1 = \theta_2 = 0$ and three non-trivial solutions [5–7]:

$$\text{(I):} \quad \theta_2 = 0, \quad p = \frac{\theta_1}{\sin\theta_1},$$

$$\text{(II):} \quad \theta_1 = 0, \quad p = \frac{c\theta_2}{\sin\theta_2}, \tag{7}$$

$$\text{(III):} \quad p = \frac{\theta_1}{\eta \sin 2\theta_1} = \frac{c\theta_2}{\eta \sin\theta_2}.$$

The critical load $p = p_{cr}$ occurs when the equilibrium path I intersects the trivial solution, so that $p_{cr} = 1$. A secondary bifurcation then is encountered on path I when it is intersected by path III. This occurs at $\theta_1 = \theta_1^*$, $\theta_2 = 0$, and $p = p^*$ where [5–7]

$$c \sin 2\theta_1^* = 2\theta_1^*, \qquad p^* = c \cos\theta_1^*. \tag{8}$$

The second of these equations is obtained by letting θ_2 approach zero in the second equation for case III in equations (7), and the first by using case I. Equilibrium paths in the (θ_1, p) plane are plotted in Figure 2 for $c = 1{\cdot}1$, in which case $p^* = 1{\cdot}024$ and $\theta_1^* = 0{\cdot}3745$. The range $0{\cdot}8 < p < 1{\cdot}1$ is shown in Figures 2–5.

To investigate small vibrations about the trivial equilibrium state, equations (6) are linearized, leading to the squared frequencies

$$\omega_A^2 = 1 - p, \qquad \omega_B^2 = c - p. \tag{9}$$

The curves of p versus ω^2 (i.e., characteristic curves) are linear and are shown in Figure 3 for $c = 1{\cdot}1$, and up to $p = 1$ (when the trivial solution becomes unstable).

For vibrations about path I, $\theta_1(t)$ and $\theta_2(t)$ in equations (7) are replaced by the sum of their equilibrium values and small motions $\phi_1(t)$ and $\phi_2(t)$, respectively, and the resulting

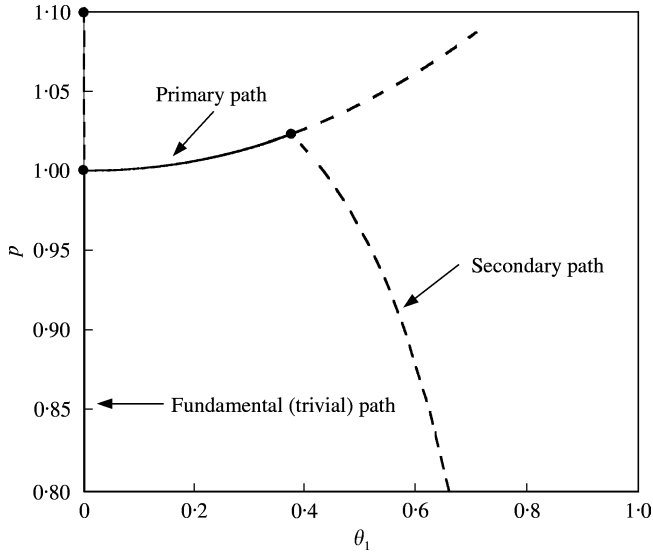

Figure 2. Equilibrium paths for the perfect system: $c = 1{\cdot}1$, $p_{cr} = 1{\cdot}0$, $p^* = 1{\cdot}024$, $\theta_1^* = 0{\cdot}3745$.

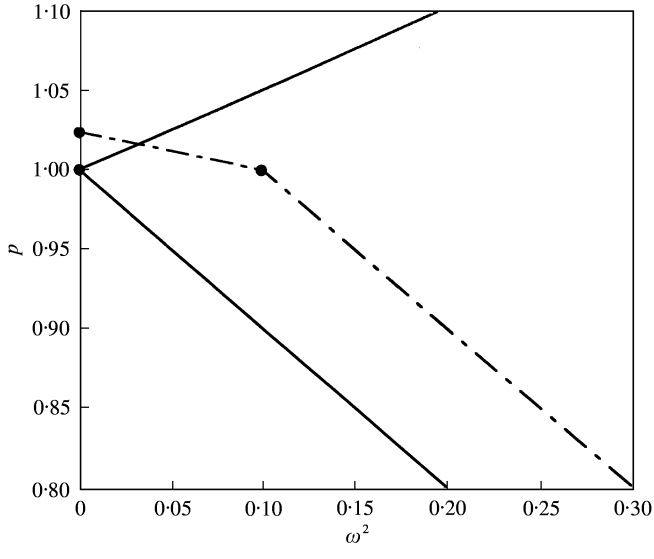

Figure 3. Characteristic curves for the perfect system: $c = 1{\cdot}1$; ——, ω_A^2; – · –, ω_B^2.

equations in $\phi_1(t)$ and $\phi_2(t)$ are linearized. The squared frequencies are found to be

$$\omega_A^2 = 1 - p\cos\theta_1 = 1 - \frac{\theta_1}{\tan\theta_1}, \qquad \omega_B^2 = c - \frac{p}{\cos\theta_1} = c - \frac{2\theta_1}{\sin 2\theta_1}. \tag{10}$$

These frequencies are applicable for $p > 1$ and are plotted in Figure 3 for $c = 1{\cdot}1$. As for vibrations about the trivial solution, the modes are uncoupled, with $\phi_2 = 0$ for the mode associated with ω_A and $\phi_1 = 0$ for the mode associated with ω_B.

The equilibrium states on path I are stable (since the squared frequencies are positive) until secondary bifurcation occurs at $p = p^*$. At that point, based on equations (8), the

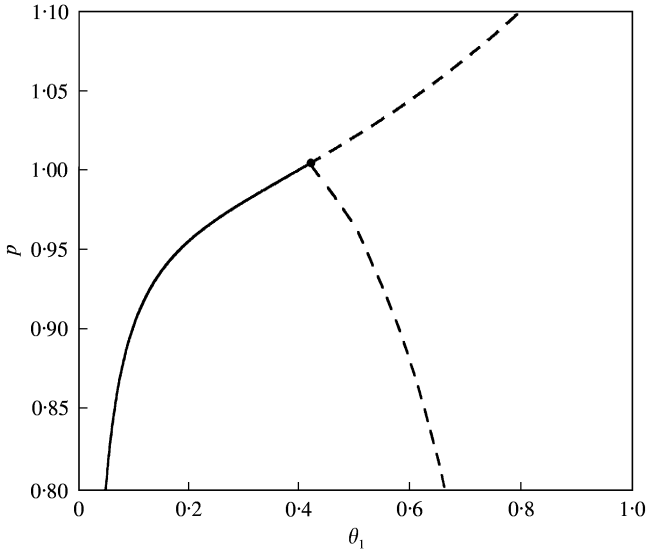

Figure 4. Equilibrium paths for the imperfect system: $c = 1{\cdot}1$, $p_b = 1{\cdot}0052$, $\theta_b = 0{\cdot}4183$, $\theta_{10} = 0{\cdot}01$, $\theta_{20} = 0{\cdot}0$.

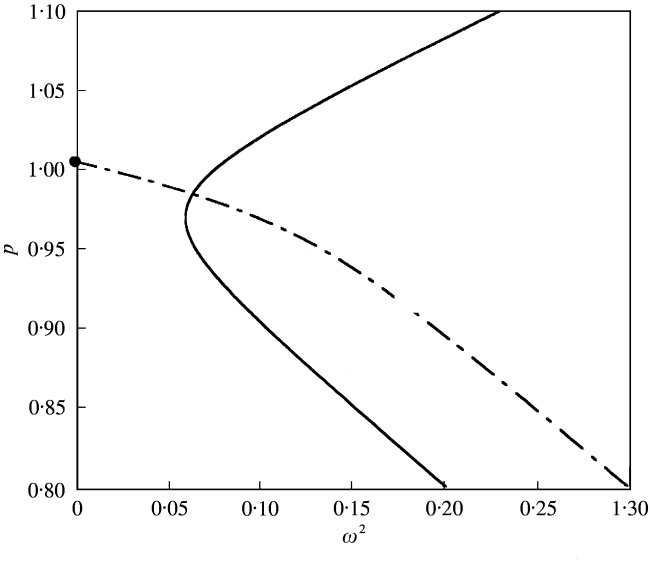

Figure 5. Characteristic curves for the imperfect system: $c = 1{\cdot}1$, $\theta_{10} = 0{\cdot}01$; ——, ω_A^2; – · –, ω_B^2.

frequency ω_B in equation (10) becomes zero. Therefore, if some values of the frequency ω_B were determined for the physical system as the load is increased, extrapolation of the characteristic curve could be used to estimate the value of p^*. If a curve fit to the data points is not almost linear, then the technique proposed in reference [1] could be applied, in which the load is plotted versus various powers of the computed values of the relevant frequency until an almost-linear relationship is found.

If the truncated analysis had been used, as in references [8–12], the equation for path I would be $p = [1 - (\theta_1^2)/6]^{-1}$, secondary bifurcation would occur when $(\theta_1^*)^2 = 6(c-1)/(c+3)$ and $p^* = (c+3)/4$, and the frequencies for path I would be

$\omega_A^2 = 2(p-1)$ and $\omega_B^2 = c + 3 - 4p$. Therefore, the characteristic curves for that approximate analysis would be composed of linear segments, whereas the exact relations are not quite linear.

4. CHARACTERISTIC CURVES FOR IMPERFECT SYSTEM

When the initial geometry of Augusti's model is not perfect, the primary equilibrium path may become unstable at a limit point or a bifurcation point, and secondary bifurcation from a stable state does not occur.

Consider a case in which $\theta_{10} > 0$ and $\theta_{20} = 0$ [4–6]. From equations (6), the primary equilibrium path is given by

$$p = \frac{\theta_1 - \theta_{10}}{\sin\theta_1}. \tag{11}$$

Bifurcation occurs when $p = p_b$, $\theta_1 = \theta_b$, and $\theta_2 = 0$, where

$$c \sin 2\theta_b = 2(\theta_b - \theta_{10}), \qquad p_b = c\cos\theta_b. \tag{12}$$

Frequencies for small vibrations about the primary path are given by equations (10) except that θ_1 in the numerator of the last expression for each frequency is replaced by $\theta_1 - \theta_{10}$.

The equilibrium and characteristic curves are plotted in Figures 4 and 5, respectively, when $c = 1{\cdot}1$ and $\theta_{10} = 0{\cdot}01$, for which $p_b = 1{\cdot}0052$ and $\theta_b = 0{\cdot}4183$. Instability can be predicted by extrapolating the frequency which is originally the higher one to the load at which it will reach zero. As seen in Figure 5, the curve for this case is almost linear as p approaches p_b.

5. DYNAMIC BEHAVIOR

The dynamic response of the model is of interest. In particular, it is enlightening to investigate the motion of the system as the load is slowly increased. A very small amount of damping is now added (0·1% in each mode for the purposes of numerical stability), so that the motions are slowly attracted to nearby stable equilibrium states. The relations governing the frequencies of small-amplitude oscillations are based on the results above. Damping has the effect of causing oscillations to cease just prior to the onset of instability [15].

Figure 6 shows a single time series based on the numerical integration of equations (6) with damping, $\theta_{10} = \theta_{20} = 0{\cdot}0$, and $c = 1{\cdot}1$. In this case, the axial load is evolved (in a slow non-stationary sense) according to the scheme

$$p = 0{\cdot}95 + 0{\cdot}00005\tau \tag{13}$$

such that the initial critical load is reached when $\tau = 1000$. Initial conditions $\theta_1(0) = \theta_2(0) = 0{\cdot}05$ generated the oscillations shown, and the gradual change in vibration frequency is observed in both time series. Under these conditions, when p passes unity (at $\tau = 1000$), the system follows the stable post-buckled solution and some more transients are generated in this buckling process. Subsequent increase in load enables the secondary bifurcation to be encountered at $\tau = 1480$ (when $p = 1{\cdot}024$). Prior to the secondary

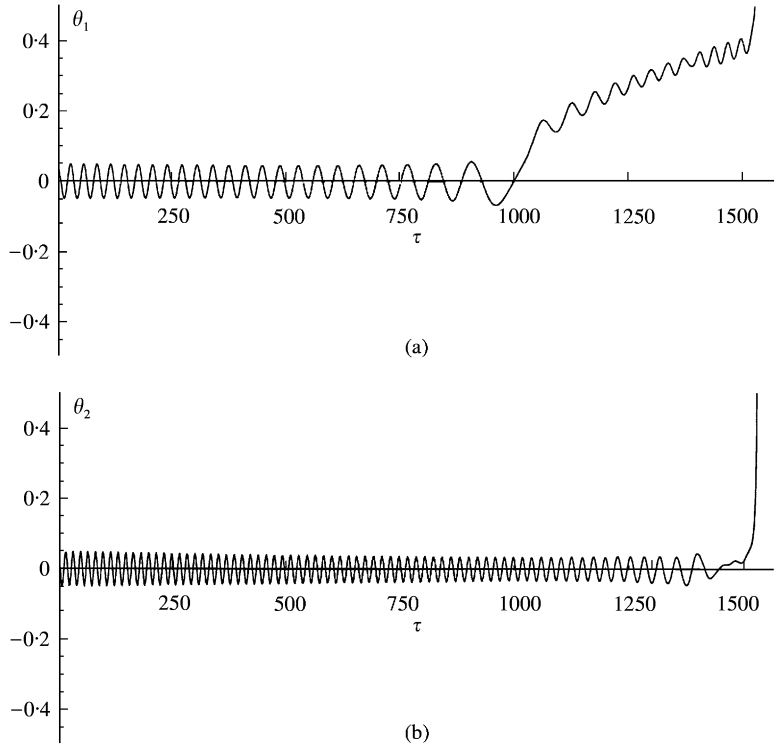

Figure 6. A time series of oscillations during a transition through initial and secondary bifurcation: $c = 1{\cdot}1$, $\theta_1(0) = \theta_2(0) = 0{\cdot}05$, $\theta_{10} = \theta_{20} = 0$, 0·1% damping; (a) θ_1, (b) θ_2.

bifurcation we observe the anticipated increase in natural frequency (the first of equations (10)) in the θ_1 direction and the *reduction* in natural frequency (the second of equations (10)) in the θ_2 direction. No stable equilibrium state exists at higher values of p, and hence the system completely loses stability. This is unlike the behavior demonstrated in references [3, 4] for which mode jumping occurs at secondary bifurcation.

6. CONCLUDING REMARKS

Secondary bifurcation on a stable equilibrium path is typically associated with instability. It has been observed as mode jumping in plates and other structural systems. This phenomenon can be predicted by extrapolating the vibration frequencies at increasing load levels to the load at which one frequency would become zero.

This proposed technique has been investigated here for Augusti's model, a two-degree-of-freedom system. If the system is perfectly straight when unloaded, it exhibits bifurcation to a stable equilibrium path, followed by secondary bifurcation (and instability). The frequency that is initially lower becomes zero at the first bifurcation point. Then one of the frequencies for small vibrations about the stable equilibrium path increases from zero, while the other decreases and becomes zero when secondary bifurcation occurs. The characteristic curve in the plot of load versus frequency squared may be almost linear as this bifurcation is approached, so that extrapolation could give an accurate prediction of the conditions for instability.

ACKNOWLEDGMENTS

The first author gratefully acknowledges the support of the Technical University of Vienna, Austria, where some of this research was conducted during a stay at the Institute for Machine Dynamics and Measurement. The authors are also grateful to Professor Giuliano Augusti for providing some of the references.

REFERENCES

1. R. H. PLAUT and L. N. VIRGIN 1990 *Journal of Engineering Mechanics* **116**, 2330–2335. Use of frequency data to predict buckling.
2. F. BLOOM and D. W. COFFIN 2001 *Handbook of Thin Plate Buckling and Post Buckling*. Boca Raton, FL: CRC Press.
3. P. R. EVERALL and G. W. HUNT 2000 *International Journal of Non-Linear Mechanics* **35**, 1067–1079. Mode jumping in the buckling of struts and plates: a comparative study.
4. H. TROGER and A. STEINDL 1991 *Nonlinear Stability and Bifurcation Theory*. Berlin: Springer-Verlag.
5. G. AUGUSTI 1964 *Ph.D. Thesis, Department of Engineering, University of Cambridge*. Some problems in structural instability, with special reference to beam-columns of I-section.
6. G. AUGUSTI 1964 *Memoria estratta dal Vol.* IV, *Series* 3*a*, *No.* 5, *degli Atti dell'Accademia delle Scienze fisische e matematiche di Napoli*. Stabilità di strutture elastiche elementari in presenza di grandi spostamenti (Stability of elastic structures in the presence of large displacements).
7. G. AUGUSTI, V. SEPE and A. PAOLONE 1998 in *Coupled Instabilities in Metal Structures: Theoretical and Design Aspects* (J. Rondal, editor), 1–27. Vienna: Springer-Verlag. An introduction to compound and coupled buckling and dynamic bifurcations.
8. J. M. T. THOMPSON and G. W. HUNT 1973 *A General Theory of Elastic Stability*. London: Wiley.
9. A. J. REIS and J. ROORDA 1979 *Journal of the Engineering Mechanics Division, American Society of Civil Engineers* **105**, 609–621. Post-buckling behavior under mode interaction.
10. M. PIGNATARO, N. RIZZI and A. LUONGO 1991 *Stability, Bifurcation and Postcritical Behaviour of Elastic Structures*. Amsterdam: Elsevier.
11. V. GIONCU 1998 in *Coupled Instabilities in Metal Structures: Theoretical and Design Aspects* (J. Rondal, editor), 85–149. Vienna: Springer-Verlag. Phenomenological and mathematical modelling of coupled instabilities.
12. L. A. GODOY 2000 *Theory of Elastic Stability: Analysis and Sensitivity*. Philadelphia: Taylor & Francis.
13. A. LUONGO and A. PAOLONE 1998 *Journal of Sound and Vibration* **218**, 527–539. Multiple scale analysis for divergence–Hopf bifurcation of imperfect symmetric systems.
14. H. YEH and J. I. ABRAMS 1960 *Principles of Mechanics of Solids and Fluids. Vol.* 1: *Particle and Rigid-Body Mechanics*. New York: McGraw-Hill.
15. L. N. VIRGIN 1986 *Journal of Sound and Vibration* **110**, 99–109. Parametric studies of the dynamic evolution through a fold.